Photonic simulation method applied to the study of structural color in *Myxomycetes*

Andrés Dolinko,[1] **Diana Skigin,**[1,*] **Marina Inchaussandague,**[1] **and Cecilia Carmaran**[2]

[1]*Grupo de Electromagnetismo Aplicado, Departamento de Física, FCEN, Universidad de Buenos Aires, and IFIBA, CONICET Ciudad Universitaria, Pabellón I, C1428EHA Buenos Aires, Argentina*

[2]*Departamento de Biodiversidad y Biología Experimental, Facultad de Ciencias Exactas y Naturales, Universidad de Buenos Aires, Ciudad Universitaria, Pabellón II, C1428EHA Buenos Aires, Argentina*

[*]*dcs@df.uba.ar*

Abstract: We present a novel simulation method to investigate the multicolored effect of the *Diachea leucopoda* (Physarales order, *Myxomycetes* class), which is a microorganism that has a characteristic pointillistic iridescent appearance. It was shown that this appearance is of structural origin, and is produced within the peridium -protective layer that encloses the mass of spores-, which is basically a corrugated sheet of a transparent material. The main characteristics of the observed color were explained in terms of interference effects using a simple model of homogeneous planar slab. In this paper we apply a novel simulation method to investigate the electromagnetic response of such structure in more detail, i.e., taking into account the inhomogeneities of the biological material within the peridium and its curvature. We show that both features, which could not be considered within the simplified model, affect the observed color. The proposed method is of great potential for the study of biological structures, which present a high degree of complexity in the geometrical shapes as well as in the materials involved.

OCIS codes: (000.1430) Biology and medicine; (160.2710) Inhomogeneous optical media; (240.0310) Thin films; (260.3160) Interference; (330.1690) Color.

References and links

1. A. Parker, "515 million years of structural colour," J. Opt. A, Pure Appl. Opt. **2**, R15-R28 (2000).
2. P. Vukusic and J. R. Sambles, "Photonic structures in biology," Nature **424**, 852-855 (2003).
3. S. Berthier, *Iridescences, the physical colours of insects* (Springer Science+Business Media, LLC, 2007).
4. S. Kinoshita, *Structural colors in the realm of nature* (World Scientific Publishing Co., 2008).
5. S. M. Doucet and M. G. Meadows, "Iridescence: a functional perspective," J. R. Soc., Interface **6**, S115-S132 (2009).
6. S. Yoshioka and S. Kinoshita, "Single-scale spectroscopy of structurally colored butterflies: measurements of quantified reflectance and transmittance," J. Opt. Soc. Am. A **23**, 134–141 (2006).
7. W. Zhang, D. Zhang, T. Fan, J. Ding, J. Gu, Q. Guo, and H. Ogawa, "Biomimetic zinc oxide replica with structural color using butterfly (Ideopsis similis) wings as templates," Bioinsp. Biomim. **1**, 89-95 (2006).
8. R. J. Martín-Palma, C. G. Pantano, and A. Lakhtakia, "Biomimetization of butterfly wings by the conformal-evaporated-film-by rotation technique for photonics," Appl. Phys. Lett. **93**, 083901 (2008).
9. R. J. Martín-Palma and A. Lakhtakia, "Biomimetics and bioinspiration," Proc. SPIE **7401**, 1–196 (2009).
10. S. Stephenson, and H. Stempen, *Myxomycetes. A handbook of slime molds* (Timber Press, 2000).

#166619 - $15.00 USD Received 16 Apr 2012; revised 22 May 2012; accepted 10 Jun 2012; published 21 Jun 2012

11. H. W. Keller, M. Skrabal, U. Eliasson, and T. Gaither, "Tree canopy biodiversity in the Great Smoky Mountains national park: ecological and developmental observations of a new Myxomycete species of Diachea," Mycologia **96**, 537–547 (2004).
12. J. D. Schoknecht and H. W. Keller, "Peridial composition of white fructifications in the trichiales (Perichaena and Dianema)," Can. J. Bot. **55**, 1807–1819 (1977).
13. H. C. Aldrich, "Influence of inorganic ions on color of lime in the myxomycetes," Mycologia **74**, 404–411 (1982).
14. T. W. Gaither and H. W. Keller, "Taxonomic comparison of *Diachea subsessilis* and *D. Deviata* (Myxomycetes, Didymiaceae) using scanning electron microscopy," Syst. Geogr. Pl. **74**, 217–230 (2004).
15. M. Inchaussandague, D. Skigin, C. Carmaran, and S. Rosenfeldt, "Structural color in *Myxomycetes*," Opt. Express **18**, 16055–16063 (2010).
16. C. Carmaran, Departamento de Biodiversidad y Biología Experimental, FCEN, University of Buenos Aires, Ciudad Universitaria, Pabellón II, C1428EHA Buenos Aires, Argentina, S. Rosenfeldt, D. Skigin, M. Inchaussandague, and H. Keller, are preparing a manuscript to be called "Iridescence and ultrastructure in the myxomycete *Diachea leucopodia* (Physarales)."
17. P. Vukusic and D. G. Stavenga, "Physical methods for investigating structural colours in biological systems," J. R. Soc., Interface **6**, S133–S148 (2009).
18. S. Kinoshita, S. Yoshioka, and J. Miyazaki, "Physics of structural colors," Rep. Prog. Phys. **71**, 076401 (2008).
19. S. Yoshioka, E. Nakamura, and S. Kinoshita, "Origin of two-color iridescence in rock dove's feather," J. Phys. Soc. Jpn. **76**, 013801 (2007).
20. J. A. Noyes, P. Vukusic, and I. R. Hooper, "Experimental method for reliably establishing the refractive index of buprestid beetle exocuticle," Opt. Express **15**, 4351-4357 (2007).
21. S. Yoshioka and S. Kinoshita, "Direct determination of the refractive index of natural multilayer systems," Phys. Rev. E **83**, 051917 (2011).
22. A. Luna, D. Skigin, M. Inchaussandague, and A. Roig Alsina, "Structural color in beetles of South America," Proc. SPIE **7782**, 778205 (2010).
23. B. Gralak, G. Tayeb, and S. Enoch, "Morpho butterflies wings color modeled with lamellar grating theory," Opt. Express **9**, 567–578 (2001).
24. R. O. Prum and R. Torres, "Structural colouration of avian skin: convergent evolution of coherently scattering dermal collagen arrays," J. Exp. Biol. **206**, 2409–2429 (2003).
25. R. O. Prum, T. Quinn, and R. Torres, "Anatomically diverse butterfly scales all produce structural colours by coherent scattering," J. Exp. Biol. **209**, 748–765 (2006).
26. A. E. Dolinko, "From Newton's second law to Huygens's principle: visualizing waves in a large array of masses joined by springs," Eur. J. Phys. **30**, 1217–1228 (2009).
27. U. Eliasson, "Ultrastructure of Lycogala and Reticularia," Trans. Br. Mycol. Soc. **77**, 243–249 (1981).
28. E. F. Haskins and M. D. McGuiness, "Sporophore ultrastructure of Echinostelium arboreum," Mycologia **81**, 303–307 (1989).
29. R. McHugh and C. Reid, "Sporangial ultrastructure of Hemitrichia minor (Myxomycetes: Trichiales)," Mycol. Res. **94**, 1144–1146 (1990).
30. A. A. Maradudin, T. Michel, A. R. McGurn, and E. R. Méndez, "Enhanced backscattering of light from a random grating," Ann. Phys. **203**, 255–307 (1990).

1. Introduction

Many natural species are known to use structural color effects to generate their appearance and visibility. Structural colors have a physical origin and are produced by the interactions of natural light with the microstructures present in the cover tissues of biological organisms. In general, color results from a combination of pigmentary and structural effects [1,2], such as interference, diffraction and scattering. The study of the interaction between the electromagnetic waves and the intricate biological structures has recently attracted the attention of biologists, physicists and engineers [3,4], since it contributes to biological sciences by identifying their behavioural functions [5] and, at the same time, natural structures inspire biomimetic technologies for applications in different industries related to color [6–9].

The *Myxomycetes* are a group of organisms that exhibit characteristics of both fungi and animals, and are considered to be more closely related to the protozoans [10]. There are some genera which exhibit bright colors, one of which is *Diachea*, which belongs to the Physarales order. In particular, *Diachea leucopoda* (Bull.) Rostaf. is characterized by a cylindrical stalked fruiting body (sporangia), with a thin, corrugated, external layer (peridium), that covers the mass of spores [11]. The color in *Myxomycetes* has been investigated due to its use as a tax-

#166619 - $15.00 USD Received 16 Apr 2012; revised 22 May 2012; accepted 10 Jun 2012; published 21 Jun 2012

onomical tool [12–14]. Previous studies on *Diachea* individuals reported that certain species exhibit beautiful bronze and/or blue iridescent colors, whereas others do not display any optical effect [14]. In a recent paper, we demonstrated that the multicolored pointillistic effect, characteristic of the *Diachea leucopoda*, is of structural origin, and it is produced by light interference within the peridium [15]. In [15], the peridium was modelled as a planar film of a homogeneous transparent material, and it was shown that the observed color depends on the layer's thickness and on the refraction index of the material. The results obtained also showed that the peridium has other interesting properties, such as autofluorescence and iridescence, which could be of high impact in ecological studies of this group of organisms, and also exhibits potential applications in industry [16].

Natural photonic structures exhibit a high degree of complexity in their geometrical shapes as well as in the materials involved. For this reason, appropriate theoretical methods must be employed, which would permit one to correctly predict and investigate the electromagnetic response of biological photonic systems [17]. The simplest model of thin film interference has been able to successfully explain the color appearance in dove feathers [18, 19]; the multilayer reflector electromagnetic model was used to explain the iridescent effect in many species, especially in the cover tissues of beetles [18,20–22]. Also, diffraction grating models have been used to reproduce the electromagnetic response of butterflies' scales [23]. For three-dimensional structures, a simple approach was adopted by Prum *et al.* [24, 25], who used two-dimensional Fourier analysis of transmission electron microscopy (TEM) images to model the effect of the periodicity in the refraction index distributions of natural structures, to predict preferent reflected wavelengths. On the other hand, there has been significant progress in electromagnetic modelling techniques for complex three-dimensional structures in the last twenty years, and this is allowing more and more precise calculations of the electromagnetic response of natural biological structures. Among these techniques, the most popular ones are finite difference time domain methods, finite element methods, and photonic bands calculation methods based on plane waves expansions. These tools require a previous and detailed definition of the exact spatial geometry and structural profiles of the modelled structure, and this task is usually done using pre-built geometrical shapes. Although this kind of methods are very useful for many systems, the appropriate design of the structure often becomes a task itself. Biological structures have intrinsically complex geometries, and therefore it is very difficult to accurately reproduce their actual shape with the available design tools.

Recently, a simple method based on the propagation of mechanical waves along a springs' mesh connecting particles of equal mass has been proposed to compute the optical response of photonic structures [26]. One of the most remarkable features of this method lies in the possibility of introducing the investigated structure (geometry and refraction index distribution) within the code by means of a digital image. This is a great advantage, especially for dealing with natural photonic structures. This method can be used to simulate electromagnetic waves' propagation along a dielectric medium (with or without absorption) in the case of a bidimensional structure (with traslational symmetry) under transverse electric (TE) incidence.

In this paper we apply a novel simulation tool proposed in [26] to investigate the electromagnetic response of *Diachea leucopoda* in more detail, taking into account the inhomogeneous nature of the peridium and its curvature. In Section 2 we summarize the simulation method, the identification of mechanical and optical parameters, and explain how the structure under study is introduced, considering its geometrical composition as well as the refraction index distribution. In Section 3 we characterize the peridium structure, and results of reflectance for different structures are shown and compared in Section 4. Finally, discussion and concluding remarks are given in Section 5.

#166619 - $15.00 USD Received 16 Apr 2012; revised 22 May 2012; accepted 10 Jun 2012; published 21 Jun 2012

2. Photonic simulation method

The simulation code developed to compute the optical response of photonic structures is based on the method presented in [26] to simulate the propagation of transverse mechanical waves. The physical system consists of a two-dimensional array of $p \times q$ particles contained in the same plane. Each particle is bonded to its four first neighbours by means of elastic springs. The movement of the particles is constrained to the direction normal to the plane of the array. To generate a wave that propagates along the plane of the particles, an external force along the transverse direction should be applied to selected particles.

For large p and q, the array of particles can be considered as a continuous medium representing an elastic membrane subjected to a tension per unit length $T = F_e/l_T$, where F_e is the elastic force and l_T is a length. The simulated membrane has a superficial mass density $\mu = mN_m/s$, where m stands for the mass of the mesh element and N_m is the number of particles contained in a region of area s. For a medium with ground density mass μ_0, the speed of the waves is given by $v_0 = \sqrt{T/\mu_0}$. Therefore, in a region with mass density $\mu > \mu_0$ the speed of the waves is $v < v_0$. Making an analogy with optics, regions with mass density μ_0 can be identified with vacuum, i.e., a medium of refraction index $n_0 = 1$, while a region with an arbitrary mass density μ corresponds to a medium with a real part of the refraction index $n = \sqrt{\mu/\mu_0}$ [26]. This approach permits to reproduce optical phenomena involving dielectric materials illuminated by transverse electric (TE) polarized light in two-dimensional configurations, and this has been verified for different systems and incidence configurations.

One of the remarkable features of this simulation method is the possibility of defining the simulation domain by means of digital images or bitmaps [26]. Each pixel of the image represents the position of the particle in the array. In this manner, a digital image of $p \times q$ pixels automatically defines the size of the simulation domain. An appropriate scale given in [nm/pixel] links the size of an object in the digital image, in pixels, with the actual physical size of the sample to be simulated, which in the case of natural photonic structures is measured in nanometers.

Three bitmaps of equal size are defined within the simulation code to introduce different characteristics of the structure and the illumination conditions, which are denoted as M (mass density), D (damping) and E (excitation). The grey levels in the M bitmap represent the mass distribution within the array, which should be assigned using an adequate linear conversion function. The bitmap D encodes the damping constant of each point of the array, which allows introducing an attenuation constant in the medium, and the E bitmap is used to specify the excitation, i.e., the particles on which the external force is applied. Following the analogy with the propagation of electromagnetic waves in an optical medium, the M bitmap determines the refraction index distribution in space, the D bitmap specifies the regions where there is absorption, and the E bitmap specifies the light sources. In this manner, this simulation method allows studying the electromagnetic response of any two-dimensional distribution of refraction index in dielectric media. This distribution can either be generated artificially, i.e., by building the structure with any available computational design tool, or by a digital image of the actual specimen to be investigated. In this paper we show results for both kinds of structures. The artificial ones allow simulating the granularity observed in the natural structures, and, at the same time, permit controlling the statistics and the general homogeneity of the synthetic slab. To generate the artificial slab, the M bitmap is defined as follows. First, the whole set of pixels is initialized with a 0 grey level (black colour). Then, a randomly selected group of pixels in this bitmap is set on a 255 grey level (full white colour). The density and the random distribution of the generated white pixels is homogeneous and it can be controlled. A convolution filter is then applied to the bitmap in order to produce a blur around the white pixels, such that the size of the convolution kernel of the filter determines the size of the blurred spots. Finally, the grey levels are linearly associated to a desired refraction index interval of known mean value. On the other

#166619 - $15.00 USD Received 16 Apr 2012; revised 22 May 2012; accepted 10 Jun 2012; published 21 Jun 2012

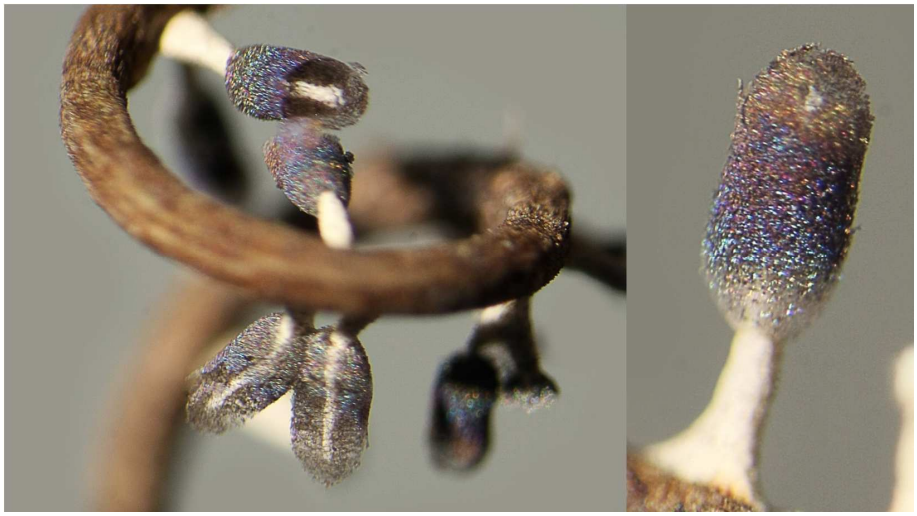

Fig. 1. *Diachea leucopoda* observed under the optical microscope.

hand, the actual structure to be analyzed is introduced into the simulation by a TEM image of the peridium cross section. Since there are no specific values of the refraction index of the *Diachea leucopoda* peridium available in the literature, its variation range was chosen according to the existing reports on refraction indices of materials comprising natural microstructures [3], as already done in [15].

3. Sample observation and characterization

In Fig. 1 we show images of fresh samples of *Diachea leucopoda* structures observed under an optical microscope. Their appearance exhibit pixels of bright colors mounted on a dark background. In these samples, areas with different hues can be distinguished, mainly orange, blue and purple. However, other samples present a pointillistic multicolor effect along the peridium surface (not shown).

Scanning (SEM) and transmission (TEM) electron microscope images of the peridium are shown in Fig. 2. A complete structure is shown in Fig. 2(a), and a small fragment of the peridium can be observed in Fig. 2(b), where it is evident that the profile of a transversal cross section follows a fairly regular array of undulations of heights of $\approx 5\mu$m, separated $\approx 10\mu$m. Figs. 2(c) and 2(d) show peridium cross section images obtained by SEM and TEM, respectively. It is evident from these images that the peridium is inhomogeneous: it presents granules of dense material on a light background. In Fig. 2(d) the external parts of the peridium appear more traslucid than the central one since the roughness of its topography reduces the optical density. The thickness of the peridium exhibits variations between 200 and 700 nm [27–29]. According to these works and to our observations in the SEM and TEM images for several samples, the peridium thickness is not uniform at different parts of the same sample, and it can be as thin as 50 nm.

#166619 - $15.00 USD Received 16 Apr 2012; revised 22 May 2012; accepted 10 Jun 2012; published 21 Jun 2012

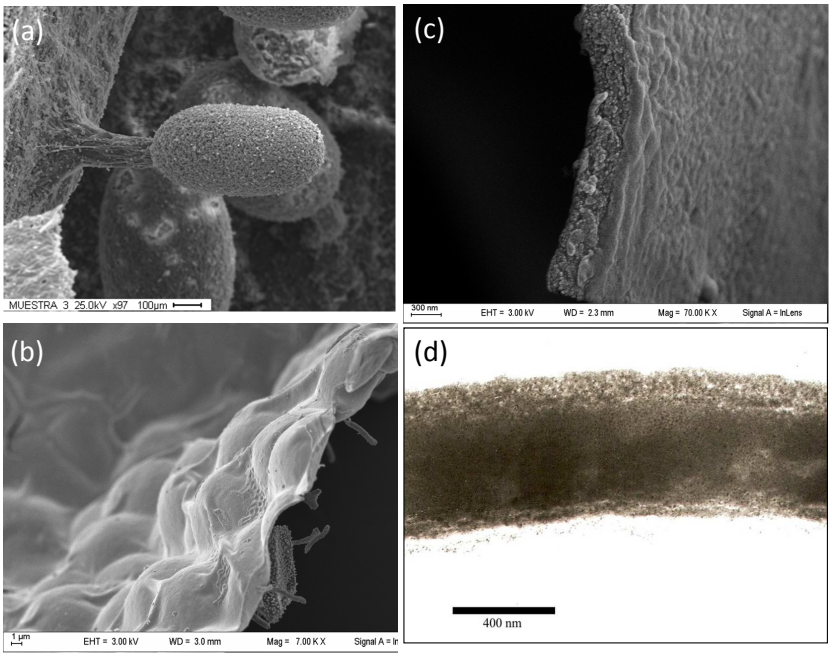

Fig. 2. (a)-(c) Scanning electron microscope images of the *Diachea leucopoda* with different magnifications: (a) a complete individual, (b) the peridium, (c) cross section of the peridium; (d) transmission electron microscope image of the peridium cross section.

4. Results

As previously observed in [14], the peridium is a transparent film, and it is the responsible of the color effect exhibited by this species, as already reported in [15]. A simple model explained that the observed color is the result of interference within a thin film (the peridium), which has non-uniform thickness. However, this model did not account neither for the influence of the inhomogeneous composition nor for the effects of the curvature in the observed color. Therefore, in this work we especially focus in these two aspects. To get insight into the influence of the inhomogeneities in the color production, in the first examples we investigate the electromagnetic response of a planar inhomogeneous slab.

In Fig. 3 we compare the total reflectance of a planar piece of peridium of 525 nm of thickness, with the reflectance of other slabs of the same thickness but different compositions. The illumination is normal to the sample and the width of the incident beam is 2 μm. The green curve corresponds to a homogeneous slab (H), the blue and the red curves correspond to artificially generated inhomogeneous slabs with the refraction index varying between 1.5 and 2 (A1), and between 1.61 and 2 (A2), respectively, and the yellow one is the reflectance from the portion of peridium (R), whose refraction index distribution has been assigned according to a TEM image of the peridium cross section. As explained in Section 2, to define the refraction index distribution, the grey levels of the bitmap of each slab are associated with a given refraction index interval of known mean value. In Fig. 3 all the slabs have been assigned the same mean value of the refraction index ($n_{mean} = 1.75$ in this example). The refraction index range was chosen according to the existing reports on refraction indices of materials comprising natural microstructures [3], which is approximately between 1.5 and 2. The bitmaps used to generate

#166619 - $15.00 USD Received 16 Apr 2012; revised 22 May 2012; accepted 10 Jun 2012; published 21 Jun 2012

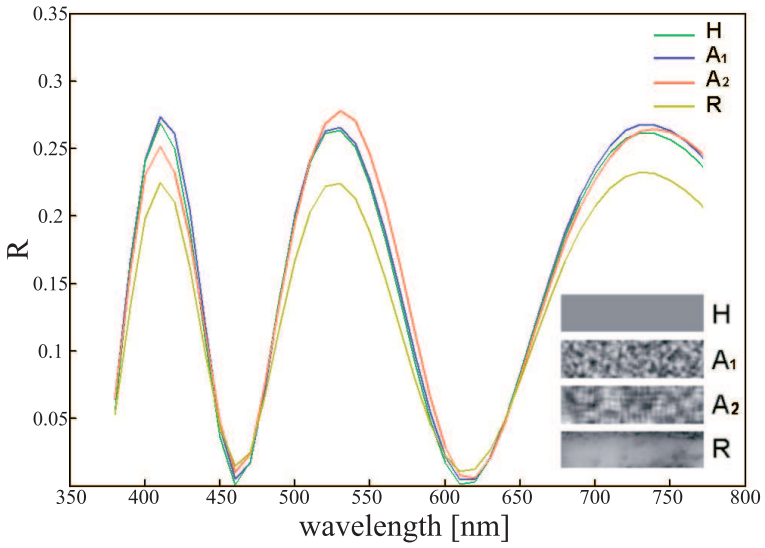

Fig. 3. Integrated reflectance of a planar slab of thickness 525 nm and $n_{mean} = 1.75$ as a function of the wavelength, for a normally incident beam of width 2μm. The different curves correspond to different compositions of the slab: homogeneous (H), inhomogeneous with $1.5 < n < 2$ and size of the granules ≈ 60 nm (A1), inhomogeneous with $1.61 < n < 2$ and size of the granules ≈ 120 nm (A2), and inhomogeneous based on a TEM image of the peridium cross section (R). Inset: bitmaps used to generate these curves. The four images share the same gray scale: black corresponds to the lower refraction index $n = 1.5$ and white to $n = 2$.

these curves are shown in the inset, where the four images share the same gray scale: black corresponds to $n = 1.5$ and white to $n = 2$. To keep the same n_{mean} in all the curves, in the case of the actual sample (curve R) the refraction index ranges between 1.5 and 1.85. Notice that the R bitmap is the complement (in terms of the grey scale) of a section of the TEM image shown in Fig. 2(d). Curves A1 and A2 also differ in the size of the granules, as observed in the inset: while in A1 the granules are of ≈ 60 nm, in A2 they are of ≈ 120 nm. For inhomogeneous slabs, the reflected light is scattered in all directions, and then, the total reflectance of the structure is obtained by integration of the angular reflection coefficient.

The four curves in Fig. 3 have peaks at the same spectral positions. This was to expect since these maxima correspond to the resonant wavelengths given by the constructive interference within the slab, that only depend on the thickness and on the mean refraction index of the slab, and both parameters are equal for all the curves. There is a noticeable difference between the actual sample and the other slabs: the granule distribution -and consequently the refraction index distribution- in samples A1 and A2 is uniform, but this is not the case in the natural TEM image, where the right zone is darker in average (lower refraction index) than the left one. This results in a slightly lower reflectance of curve R, compared with the other ones. Curves H and A1 are almost completely overlapped, and this confirms that for sizes of the granules as small as 60 nm, the integrated reflectance is not significantly affected by the inhomogeneous composition of the slab. If the granule size is increased (red curve, A2), the reflectance is slightly modified. This suggests that if the size of the inhomogeneities is kept small compared with the wavelength, the total reflectance of a planar slab is not significantly affected, and the simple model of a homogenous slab can still be used to calculate the total reflectance. However, as we shall see in the following figure, the angular distribution of intensity changes, and this

#166619 - $15.00 USD Received 16 Apr 2012; revised 22 May 2012; accepted 10 Jun 2012; published 21 Jun 2012

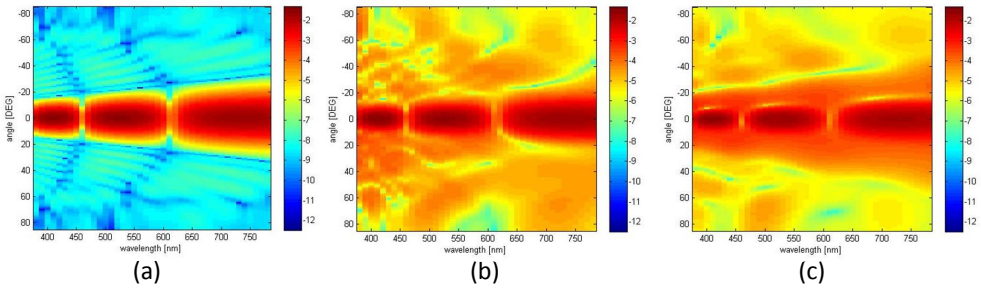

Fig. 4. Logarithm of the differential reflection coefficient of a planar slab of thickness 525 nm as a function of the wavelength and of the observation angle for a normally incident beam of width 2μm, and for three of the slabs considered in Fig. 3: (a) H; (b) A1; (c) R.

contributes to the iridescence.

To analyze the iridescent effect produced by the peridium of the *Diachea leucopoda*, in the following examples we compare the angular behaviour of the reflectance, for the different slabs. For better visualization, we plot the logarithm of the differential reflection coefficient (drc), i.e., the fraction of the total energy incident on the structure that is scattered into an angular interval about the reflection direction defined by the observation angle [30]. In Fig. 4 we show contour plots of log(drc) as a function of the wavelength and of the observation angle, for three of the slabs considered in Fig. 3: H, A1 and R. It can be noticed that for the homogeneous slab, the reflected intensity is almost completely concentrated within the original beam width, whereas for the real and for the artificially generated inhomogeneous slabs, the intensity is more spread out. As observed in Figs. 4(b) and 4(c), the intensity of light scattered in non specular directions depends on the wavelength, and this effect contributes to the iridescence, i.e., to the dependence of the observed color on the observation angle.

Up to now, only the effects of the composition of the slab has been analyzed. However, the curvature of the sample also produces iridescence and affects the observed color. Therefore, in Fig. 5 we show contour plots of the logarithm of the differential reflection coefficient for curved samples. The radius of curvature of the analyzed structures is 6 μm, and this value was taken from the SEM images of the peridium. In the case of a curved homogeneous slab (Fig. 5(a)), the reflected light is scattered back and propagates in a broad beam, much wider than that corresponding to the planar homogeneous slab (see Fig. 4(a)). If an inhomogeneous composition of the slab is also considered, the reflected intensity is modified, and the angular intensity distribution strongly depends on the wavelength, as observed in Fig. 5(b). This plot clearly shows that the curvature of the sample plays an important role in the iridescent effect observed in the *Diachea leucopoda*, and also, the inhomogeneous composition of the peridium affects the reflected intensity.

To better visualize the dependence of the reflected intensity distribution on the incident wavelength, in the movie of Fig. 6 (Media 1) we show the reflected near field intensity as the incident wavelength is increased from 380 to 780 nm. It can be observed that there are wavelengths for which the intensity is minimum, and this values correspond to the minima of the integrated reflectance shown in Fig. 3, i.e., to 460 and 620 nm, approximately. Notice that certain wavelengths are more widely scattered than others, and this produces a remarkable iridescent effect.

#166619 - $15.00 USD Received 16 Apr 2012; revised 22 May 2012; accepted 10 Jun 2012; published 21 Jun 2012

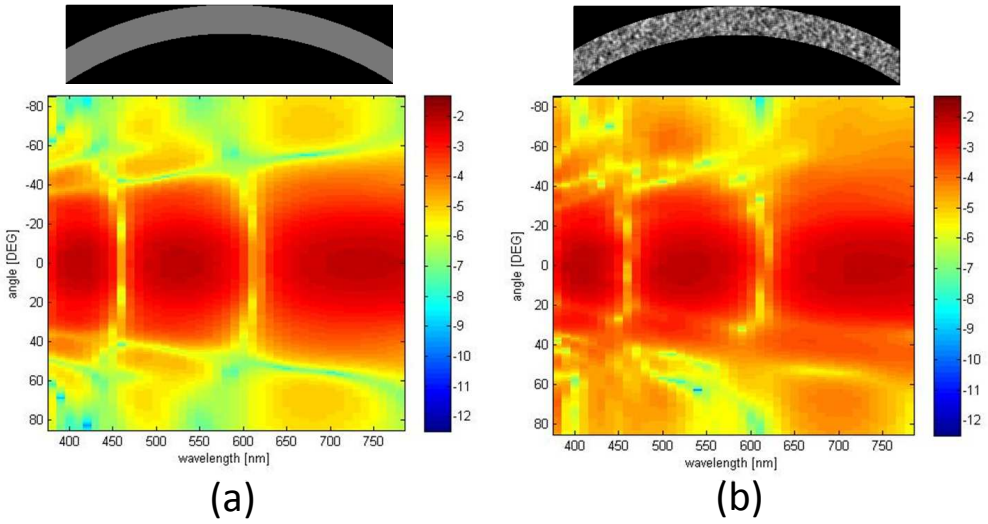

Fig. 5. Logarithm of the differential reflection coefficient of a curved slab of thickness 525 nm and radius of curvature 6 μm as a function of the wavelength and of the observation angle for a normally incident beam of width 2μm, and for different composition of the slabs. (a) homogeneous with $n = 1.75$; (b) inhomogeneous with $n_{mean} = 1.75$ and $1.5 < n < 2$. In the inset above each panel we show the corresponding refraction index bitmaps of the curved slabs.

5. Discussion

The characteristic multicolored effect exhibited by *Diachea leucopoda* was studied using a numerical simulation code especially suitable for dealing with natural photonic structures. The inhomogeneous composition as well as the curvature of the peridium have been taken into account within the model, and this allows a more realistic approach to the electromagnetic response of the actual natural system. The effects of the inhomogeneous composition of the peridium and of its curvature on the reflected response have been analyzed, and it was shown that these characteristics affect the reflectance, and consequently, the observed color.

The developed numerical method was shown to be effective for the calculation of the electromagnetic response of this complex structure. Taking into account that it permits the introduction of the structure via a digital image, this method emerges as a promising candidate for investigating structural color and other electromagnetic effects in biological structures, which are intrinsically complex in their geometrical shapes as well as in their composition.

However, in order to optimize the tool for these kind of calculations, several aspects of the method should be improved. First of all, the computation of the response under transverse magnetic (TM) polarized illumination should be included, to allow the calculation of the complete response, and reproduce the observed color. The propagation of a TM electromagnetic wave cannot be simulated by a mechanical wave in an array of particles joined by springs. Therefore, a full vectorial version of the code for the simulation of electromagnetic waves propagation is required. Second, the materials comprising biological structures usually absorb part of the incident radiation, and this is accounted for by a complex refraction index. Due to the characteristics of the *Diachea leucopoda* peridium, in this example real indices have been considered to explain the color generation in this species. However, in most natural structures color results

#166619 - $15.00 USD Received 16 Apr 2012; revised 22 May 2012; accepted 10 Jun 2012; published 21 Jun 2012

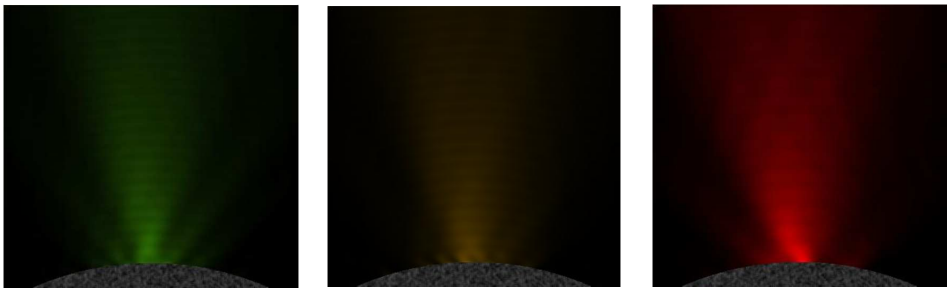

Fig. 6. Movie of the reflected near field of an artificially inhomogeneous curved slab of thickness 525 nm, radius of curvature 6 μm, $n_{mean} = 1.75$ and $1.5 < n < 2$, for a normally incident beam of width 2μm, for increasing wavelengths (from 380 to 780 nm, in steps of 10 nm) (Media 1). The three panels correspond to different frames for particular wavelengths: (a) $\lambda = 520$ nm; (b) $\lambda = 560$ nm; (c) $\lambda = 760$ nm.

from a combination of structural effects and selective absorption, and therefore the introduction of the imaginary part of the refraction index is needed in order to get an accurate response. Finally, although certain types of natural photonic structures can be accurately modelled by two-dimensional systems, biological structures are in general three-dimensional, and then, an extension of the calculation model to deal with such complex structures, with refraction index variations in all directions, still remains a challenge. The development of such an extension would permit us to analyze structures with no traslational symmetry. All these aspects are being analyzed and an improved version of the photonic simulation method is being developed.

Acknowledgments

A. D., D. S. and M. I. acknowledge partial support from Consejo Nacional de Investigaciones Científicas y Técnicas (CONICET PIP 112-200801-01880) and Universidad de Buenos Aires (UBA-20020100100533).

#166619 - $15.00 USD Received 16 Apr 2012; revised 22 May 2012; accepted 10 Jun 2012; published 21 Jun 2012